Sensitivity of Lithium-Ion Battery SOP Estimates to Sensor Measurement Error and Latency

Gregory L. Plett * Gavin McVeigh **

* University of Colorado Colorado Springs, Colorado Springs, CO USA
(e-mail: gplett@uccs.edu).

** Dukosi Ltd., Edinburgh, Scotland (e-mail:
gavinmcveigh@dukosi.com)

Abstract: Accurate estimates of cell state of power (SOP) are critical to maximize battery-pack performance and safety. Since SOP is not directly measurable, algorithms having varying complexity are implemented to compute SOP estimates. Input to these algorithms are the cell's measurable quantities, acquired with sensors whose characteristics are defined by precision, accuracy, and synchronicity. This paper provides an evaluation of the performance of SOP estimation algorithms versus the integrity of the measurements provided by the cell voltage, current, and temperature sensors. Overviews of state-of-charge and cell-resistance estimation, required by SOP, are also shown. We employ model-based simulation to compare the ideal case having zero sensor measurement error against real-life sensor performances which exhibit measurement offset, noise and nonsynchronicity. We consider typical usage scenarios in electric-vehicle and ESS applications, cell chemistry, estimation method, and sensor performance.

Keywords: battery, SOP estimation, sensor accuracy, synchronization, electric vehicle, energy storage

1. INTRODUCTION

Battery-management systems (BMS) must compute realtime estimates of the level of power a cell can sustain over a future time horizon, termed state of power (SOP), relying on measurements of voltage, current, and temperature. The research question that we address in this paper is: How do SOP estimates depend on sensor total measurement error (TME) and synchronization error when using totalleast-squares (TLS) methods to make the underlying cellresistance estimates and the bisection algorithm to estimate SOP? (Prior papers in this series ask similar questions relating to state-of-charge (SOC) and state-of-health (SOH) estimates: Plett and McVeigh (July 2024a,b).) Despite the importance of this question, we are unaware of literature that addresses it systematically. The closest paper we could find was Zeng et al. (2023), which considers sensitivity of capacity estimates to random sensor faults, not to measurement and synchronization error.

We use a simulation approach (cf. Fig. 1). We first create a synthetic "truth" dataset by simulating an equivalent-circuit model (ECM) for different scenarios. We then add measurement and synchronization errors to the truth outputs. The modified data are used as input to SOC-and SOH-estimation methods, leading to equivalent-series resistance estimates, \hat{R}_0 . The \hat{R}_0 values are used with bisection to estimate SOP. We evaluate results by comparing estimated SOP to truth SOP from the original simulation.

2. SIMULATION APPROACH

The simulation approach for generating the dataset on which the SOH estimators are evaluated is discussed in

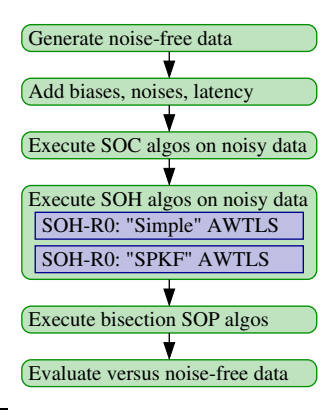


Fig. 1. Flowchart of the simulation-based strategy.

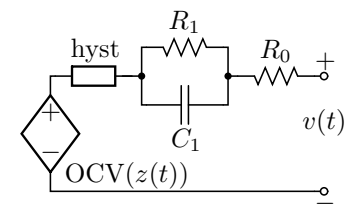


Fig. 2. An ESC-type ECM having a single resistor—capacitor "Voigt" network.

detail in Plett and McVeigh (July 2024a). Due to space constraints, we present only the most relevant details here.

The dataset was generated by simulating "enhanced-self-correcting" (ESC) ECMs per Plett (2015a) (cf. Fig. 2). In this model, cell SOC z_k is modeled as:

$$z_{k+1} = z_k - (\Delta t/Q)i_k,\tag{1}$$

where Δt is the sampling period in seconds and Q is cell total capacity in ampere-seconds (the sign convention assumes discharge current is positive and charge current is negative). Voltage of capacitor C_i is modeled as:

 $v_{c_i,k+1} = \exp(-\Delta t/\tau) v_{c_i,k} + R_i (1 - \exp(-\Delta t/\tau)) i_k,$ (2) where τ is the R–C time constant in seconds and R_i is the value of the resistor in the R-C pair in ohms. Dynamic hysteresis fraction is modeled as:

$$h_{k+1} = \exp\left(\frac{i_k\gamma\Delta t}{Q}\right)h_k - \left(1 - \exp\left(\frac{i_k\gamma\Delta t}{Q}\right)\right)\operatorname{sgn}(i_k), \ (3)$$
 where γ is a hysteresis rate factor. Cell voltage is then:

$$v_k = \text{OCV}(z_k) + Mh_k - \sum_i v_{c_i,k} - i_k R_0.$$
 (4)

where $OCV(\cdot)$ is the open-circuit voltage of the cell at a given SOC, M is the hysteresis maximum magnitude, and R_0 is the cell's equivalent-series resistance. Note that the model can support multiple R–C branches ("Voigt" networks) if we implement individual values of R_i and C_i for each R-C pair in Eq. (2).

The simulation models incorporated three R-C Voigt networks, and the SOC-estimation methods instead used models of the same cells having only two Voigt networks to account for realistic truth/model mismatch. The models used in this study were generated using data collected in the laboratory from A123 lithium-iron-phosphate (LFP) cells and Panasonic nickel-manganese-cobalt oxide (NMC) cells using the methods presented in Plett (2015a).

Automotive applications are represented via an urban dynamometer driving schedule (UDDS) profile and energystorage applications are represented via a fast frequency response (FFR) profile. Eight test cases per scenario investigated the sensitivity of results to algorithm initialization. For each scenario/test-case combination, we simulated the ECM using noise-free inputs and a sampling rate of 100 Hz.

After creating the noise-free dataset, dc biases and pseudorandom Gaussian noises were added to the current, voltage, and temperature variables per different sensor TME specifications. The voltage measurements were shifted with respect to the current and temperature measurements per different sensor synchronization specifications.

Table 1 summarizes the simulation-study settings. Table 2 itemizes the eight simulation cases considered for each scenario. Table 3 lists the assumed sensor specifications derived from publicly available datasheets. SOC estimates were made using sigma-point Kalman filters (SPKF) tuned to each scenario per Plett (2015b).

3. RESISTANCE ESTIMATION METHODS

SOP estimates rely on estimates of cell resistance. Here, we consider two TLS-based approaches from Plett and McVeigh (July 2024b), which we review below.

3.1 Method 1: The "simple method"

Consider the ECM's discrete-time voltage equation, Eq. (4). One approach to estimating R_0 is to subtract voltages at two adjacent time samples, per Plett (2015b):

$$\begin{aligned} v_k &= \text{OCV}(z_k) + M h_k - \sum_i v_{c_i,k} - i_k R_0 \\ v_{k-1} &= \text{OCV}(z_{k-1}) + M h_{k-1} - \sum_i v_{c_i,k-1} - i_{k-1} R_0 \\ v_k - v_{k-1} &\approx R_0 \left(i_{k-1} - i_k \right), \end{aligned}$$

Table 1. Simulation-study parameter settings.

Test parameter	Parameter settings
Scenarios Temperature Cases	{UDDS for NMC and LFP; FFR for LFP} {25 °C (ambient)} {z_0 initialization error of $\pm 1 \%$ }, { Q initialization error of $\pm 1 \%$ }, {truth data simulated using model having 3 R–C pairs and SPKF SOC estimates made based using model having 2 R–C pairs} The eight
Sensor models	cases of Table 2 span these conditions. dc bias and random error specified for seven sensors in Table 3.
Sensor latencies	$\{0\mathrm{ms},\pm10\mathrm{ms}\}$ between V and I

Table 2. The eight pseudo-random sim cases.

Category \ Case	1	2	3	4
Init. SOC-est. error	-1%	-1%	-1%	-1%
Capacity estimate	Q/0.99	Q/0.99	Q/0.99	Q/0.99
Current-sensor bias	$-\max$	$-\max$	$-\max$	$-\max$
Voltage-sensor bias	$+ \max$	$+ \max$	$-\max$	$-\max$
Tempsensor bias	$+ \max$	$-\max$	$+\max$	$-\max$
Category \ Case	5	6	7	8
Category \ Case Init. SOC-est. error	5 +1%	6 +1%	7 +1%	8 +1%
			•	
Init. SOC-est. error	+1,%	+1 %	+1%	+1 %
Init. SOC-est. error Capacity estimate	$+1\% \\ 0.99Q$	$+1\% \\ 0.99Q$	$+1\% \\ 0.99Q$	$+1\% \\ 0.99Q$

Table 3. Sensor TME settings for the studies.

Sensor	Label	Parameter	Vehicle setting	ESS setting		
Voltage	SV1	dc bias noise 1σ	$\begin{array}{c} 0.35\mathrm{mV} \\ 142\mu\mathrm{V} \end{array}$	$\begin{array}{c} 0.35\mathrm{mV} \\ 142\mu\mathrm{V} \end{array}$		
	SV2	dc bias noise 1σ	$\begin{array}{c} 3.5\mathrm{mV} \\ 1.5\mathrm{mV} \end{array}$	$3.5\mathrm{mV}$ $1.5\mathrm{mV}$		
	SI1	dc bias noise 1σ	$0.284 \times 10^{-3} \\ 0.130 \times 10^{-3}$	$0.071 \times 10^{-3} \\ 0.0325 \times 10^{-3}$		
Current (C-rate)	SI2	dc bias noise 1σ	$^{4.2\times10^{-3}}_{0.07\times10^{-3}}$	$\begin{array}{c} 1.05 \times 10^{-3} \\ 0.0175 \times 10^{-3} \end{array}$		
	SI3	dc bias noise 1σ	$^{18\times10^{-3}}_{24\times10^{-3}}$	$\substack{4.5 \times 10^{-3} \\ 6 \times 10^{-3}}$		
Temp.	ST1	dc bias noise 1σ	0.4°C 0.013°C	0.4 ° C 0.013 ° C		
· -F·	ST2	dc bias noise 1σ	5 ° C 0.013 ° C	5 ° C 0.013 ° C		

where we use our knowledge that that cell SOC, diffusion voltages, and hysteresis change slowly relative to i_k . So, we can formulate the R_0 -estimation problem as:

$$\underbrace{v_k - v_{k-1}}_{y} = R_0 \underbrace{i_{k-1} - i_k}_{x}, \tag{5}$$

which has the linear form $y = R_0 x$. By noting that both y and x have measurement errors, we recognize that this is a TLS problem and not a standard ordinary-least-squares problem. So, we use approximate weighted total least squares (AWTLS) method from Plett (2011) to estimate R_0 based on this model. We call this the "simple" method.

To implement the method, the variable x at any timestep is simply the difference in current between the prior and present timestep and the variable y is the difference between the present and prior voltages. Assuming that

measurement noise is white, σ_x^2 is set to twice the variance of the current-sensor random error and σ_y^2 is set to twice the variance of the voltage-sensor random $\rm \tilde{e}rror.$

3.2 Method 2: The "SPKF method"

 R_0 estimates from the "simple method" lose quality as $i_{k-1} - i_k \rightarrow 0$ and lose meaning if voltage/currentsensor synchronization is inexact. An alternate method can improve estimates, using on signals produced by the SPKF state estimator from Plett and McVeigh (July 2024a).

The "SPKF method" is developed from the cell voltage equation, replacing true quantities with their estimates from the SPKF, denoted by the "hat" symbol (•):

$$\hat{v}_k = \text{OCV}(\hat{z}_k) + M\hat{h}_k - \sum_i \hat{v}_{c_i,k} - i_k^{\text{meas}} R_0, \quad (6)$$

where $\hat{v}_{c_i,k} = R_i \hat{i}_{R_i,k}$ from the estimator. Rearranging,

$$\underbrace{-\left(\hat{v}_k - \text{OCV}(\hat{z}_k) - M\hat{h}_k + \sum_i \hat{v}_{c_i,k}\right)}_{y} = R_0 \underbrace{i_k^{\text{meas}}}_{x}, \quad (7)$$

where we once again see the linear structure $y = R_0 x$, and where both y and x have noises associated.

To implement a TLS estimator using this relationship, we exported \hat{z}_k , \hat{h}_k , and $\hat{v}_{c_i,k}$ from the SPKF state estimator, along with their covariances $\sigma_{z,k}^2$, $\sigma_{h,k}^2$, and $\sigma_{v_{c_i,k}}^2$. Computing y is straightforward and x is simply the measured current and no computation is needed to find its value.

The variance σ_x^2 needed by the TLS method is set to the

current-sensor variance
$$\Sigma_w^2$$
 tuned to optimize the SPKF. The time-varying variance $\sigma_{y,k}^2$ is computed as:
$$\sigma_{y,k}^2 = \sigma_v^2 + \left(\frac{\operatorname{d}\operatorname{OCV}(\hat{z}_k)}{\operatorname{d}\hat{z}_k}\right)^2 \sigma_{z,k}^2 + M^2 \sigma_{h,k}^2 + \sum_i \sigma_{v_{c_i},k}^2,$$

where $\sigma_v^2 = \Sigma_{\tilde{v}}$, the voltage-sensor variance tuned to optimize the SPKF. This computation assumes that the uncertainties are uncorrelated (unlikely to be true in general).

Summarizing, the "SPKF method" estimates R_0 using an alternate TLS approach. Again, we used AWTLS.

4. SOP ESTIMATION

We compute estimates of maximum dis/charge power such that cell voltage over a future time horizon of Tsamples will not exceed the range $[v_{\min}, v_{\max}]$ and cell SOC will not exceed the range $[z_{\min}, z_{\max}]$. We assume a mathematical model of cell dynamics in a discrete-time state-space form (Chen, 1999):

$$x_{k+1} = f(x_k, i_k) \tag{8}$$

$$v_k = g(x_k, i_k), \tag{9}$$

where $x_k = \begin{bmatrix} z_k & v_{c,k}^T & h_k \end{bmatrix}^T$ is the system's "state" and $f(\cdot)$ and $g(\cdot)$ are functions chosen to model the cell dynamics (i.e., $f(\cdot)$ combines Eqs. (1), (2), and (3), and $g(\cdot)$ is given by Eq. (4)). We can use this model to predict cell voltage Tsamples into the future by $v_{k+T} = g(x_{k+T}, u_{k+T})$, where x_{k+T} may be found by simulating Eq. (8) for T time samples. We assume that the input i_k remains constant from time index k to k + T.

We use the method from Plett (2004), which computes discharge and charge current limits based on $[v_{\min}, v_{\max}]$, $i_{\max}^{\text{dis,volt}}$ and $i_{\min}^{\text{chg,volt}}$, by searching for the i_k that solves

$$v_{\min} = g(x_{k+T}, i_{k+T}), \text{ or } 0 = g(x_{k+T}, i_{k+T}) - v_{\min}$$
 (10)

to find $i_{\text{max}}^{\text{dis,volt}}$, and by looking for the i_k that solves

$$v_{\text{max}} = g(x_{k+T}, i_{k+T}), \text{ or } 0 = g(x_{k+T}, i_{k+T}) - v_{\text{max}}$$
 (11)

to find $i_{\min}^{\text{chg,volt}}$. When Eq. (8) is linear, as it is with the ESC model for a constant input i_k , we can write it as $x_{k+1} = Ax_k + Bi_k$ where A and B are constant matrices. Then, for i_k constant from time k to k+T, we have

$$x_{k+T} = A^T x_k + \left(\sum_{j=0}^{T-1} A^{T-1-j} B\right) i_k.$$

Most of these terms may be pre-computed without knowledge of i_k to speed the search.

We compute current limits based on $[z_{\min}, z_{\max}]$ as:

$$i_{\text{max}}^{\text{dis,soc}} = Q \left(z_k(t) - z_{\text{min}} \right) / (T \Delta t)$$
 (12)

$$i_{\min}^{\text{chg,soc}} = Q \left(z_k(t) - z_{\max} \right) / (T\Delta t). \tag{13}$$

Overall current limits may be computed as

$$i_{\text{max}}^{\text{dis}} = \min\left(i_{\text{max}}, i_{\text{max}}^{\text{dis,soc}}, i_{\text{max}}^{\text{dis,volt}}\right)$$
 (14)

$$i_{\min}^{\text{chg}} = \max \left(i_{\min}, i_{\min}^{\text{chg,soc}}, i_{\min}^{\text{chg,volt}} \right),$$
 (15)

where battery-pack electronics require that i_k remain in $[i_{\rm min},i_{\rm max}].$ Signed SOP estimates are then calculated as

$$P_{\min}^{\text{chg}} = i_{\min}^{\text{chg}} g(x_{k+T}, i_{\min}^{\text{chg}})$$

$$P_{\max}^{\text{dis}} = i_{\max}^{\text{dis}} g_k(x_{k+T}, i_{\max}^{\text{dis}}).$$

Bisection search: To solve (10) and (11) we require a method to solve for a root of a nonlinear equation. Here, we use the bisection search algorithm to do so (Press et al., 1992). This method looks for a root of f(x) (i.e, a value of x such that f(x) = 0) where it is known a priori that the root lies between values $x_1 < root < x_2$. One way of knowing that a root lies in this interval is that the sign of $f(x_1)$ is different from the sign of $f(x_2)$.

Each iteration of the bisection search evaluates the function at the midpoint $x_{\text{mid}} = (x_1 + x_2)/2$. Based on the sign of the evaluation, either x_1 or x_2 is replaced by x_{mid} to retain different signs on $f(x_1)$ and $f(x_2)$, halving the uncertainty in the root location. The algorithm repeats this iteration until the interval $|x_2 - x_1|$ is as small as desired. If ε is the desired root resolution, then the algorithm will require at most $\lceil \log_2(|x_2 - x_1|/\varepsilon) \rceil$ iterations.

Finding maximum/minimum current: Bisection is incorporated in the overall algorithm as follows. First, three simulations are performed to determine cell voltages Tsamples into the future for cell current $i_k = 0$, $i_k = i_{\min}$, and $i_k = i_{\text{max}}$. If cell voltages are predicted to be between v_{\min} and v_{\max} for the maximum dis/charge rates, then these maximum rates may be used. If the cell voltages, even during rest, are outside of bounds, then set the maximum rates to zero. Otherwise, we know that the true maximum rate may be found by bisecting between rate equal to zero and its maximum value. Bisection is performed between current limits $(i_{\min}, 0)$ or $(0, i_{\max})$.

 $^{^{1}\,}$ Note that these are signed quantities, so maximum absolute charge current corresponds to minimum signed charge current.

Table 4. R_0 -estimate results using the simple and SPKF methods. Columns tabulate normalized RMSE in percent and percent of time that true resistance is outside the estimator's confidence bounds. Entries denoted '—' represent values that are too large to display in the table.

					Laten	cy = -101	ms (value	s in (%))	Latency = $0 \mathrm{ms}$ (values in (%))				Latency = $10 \mathrm{ms}$ (values in (%))			
					Simple	Simple	SPKF	SPKF	Simple	Simple	SPKF	SPKF	Simple	Simple	SPKF	SPKF
SI	SV	ST	Profile	Cell	RMSE	Bounds	RMSE	Bounds	RMSE	Bounds	RMSE	Bounds	RMSE	Bounds	RMSE	Bounds
			UDDS	NMC	99.92	100.00	1.55	0.00	0.04	0.00	1.52	0.00	100.01	100.00	1.60	0.00
1	1	1	UDDS	$_{ m LFP}$	99.87	100.00	3.40	3.17	0.06	0.00	3.43	3.72	99.97	100.00	3.30	2.82
			FFR	LFP	99.76	100.00	2.56	0.00	0.11	0.00	3.63	0.00	99.84	100.00	2.60	0.00
			UDDS	NMC	99.77	100.00	7.34	0.00	0.39	4.43	7.35	0.00	99.96	100.00	7.33	0.00
1	2	2	UDDS	$_{ m LFP}$	99.93	100.00	8.59	0.00	0.56	0.00	8.61	0.00	99.92	100.00	8.55	0.00
			FFR	LFP	100.12	100.00	24.29	0.00	0.87	0.00	24.82	0.00	99.87	100.00	24.27	0.00
2	1	1	FFR	LFP	99.76	100.00	12.72	0.00	0.11	0.00	15.01	0.00	99.84	100.00	12.64	0.00
2	2	2	FFR	LFP	100.12	100.00	25.85	0.00	0.87	0.00	26.61	0.00	99.87	100.00	25.82	0.00
	-1	-1	UDDS	NMC	_	0.00	2.18	0.15	0.18	0.00	2.18	0.00	_	0.00	2.22	1.69
3	1	1	UDDS	LFP	_	0.64	29.65	0.00	0.18	0.00	29.69	0.00	_	0.20	29.57	0.00
			UDDS	NMC	99.66	100.00	8.06	0.00	0.56	1.56	8.05	0.00	99.82	100.00	8.07	0.00
3	2	2	UDDS	$_{ m LFP}$	100.14	100.00	11.54	0.00	0.99	6.73	11.53	0.00	100.02	100.00	11.56	0.00
			FFR	LFP	99.91	100.00	31.62	0.00	1.02	0.02	30.86	0.00	99.66	100.00	31.65	0.00

Table 5. SOP-estimate results based on $\hat{R}_0 + 3\sigma_{R_0}$ from the simple and SPKF methods. Columns tabulate percent normalized RMSE and percent of time that SOP estimates exceed true SOP.

					Latenc	y = -101	ms (value	s in (%))	Latency = 0ms (values in (%))				Latency = $10 \mathrm{ms}$ (values in (%))			
					Simple	Simple	SPKF	SPKF	Simple	Simple	SPKF	SPKF	Simple	Simple	SPKF	SPKF
SI	SV	ST	Profile	Cell	RMSE	overest	RMSE	overest	RMSE	overest	RMSE	overest	RMSE	overest	RMSE	overest
			UDDS	NMC	232.60	99.85	6.32	0.00	1.12	2.02	6.33	0.00	233.27	99.85	6.30	0.00
1	1	1	UDDS	LFP	192.17	99.96	7.79	0.24	1.71	99.35	7.81	0.22	192.69	99.96	7.75	0.25
			FFR	LFP	205.06	100.00	12.73	0.00	1.67	99.94	14.12	0.00	205.52	100.00	12.68	0.00
			UDDS	NMC	223.89	99.84	21.08	0.00	3.51	13.75	21.10	0.00	225.18	99.84	21.05	0.00
1	2	2	UDDS	LFP	185.04	99.82	36.53	0.00	2.20	78.01	36.54	0.00	184.87	99.83	36.50	0.00
			FFR	LFP	192.37	99.95	84.92	0.00	1.97	60.95	84.97	0.00	191.22	99.96	84.91	0.00
2	1	1	FFR	LFP	204.75	100.00	69.89	0.00	1.56	99.94	70.11	0.00	205.21	100.00	69.88	0.00
2	2	2	FFR	LFP	192.22	99.95	76.18	0.00	1.98	59.15	76.32	0.00	191.07	99.96	76.18	0.00
	1	-	UDDS	NMC	104.77	0.33	6.35	0.02	5.59	0.46	6.36	0.01	100.10	0.12	6.33	0.03
3	1	1	UDDS	LFP	107.18	0.20	79.14	0.00	9.15	50.43	79.14	0.00	99.78	0.06	79.14	0.00
			UDDS	NMC	223.09	99.91	16.98	0.00	10.43	17.91	16.96	0.00	223.96	99.91	16.97	0.00
3	2	2	UDDS	$_{ m LFP}$	186.19	99.87	37.31	0.00	3.33	65.86	37.32	0.00	185.34	99.87	37.28	0.00
			FFR	LFP	191.05	99.94	67.42	0.00	2.14	61.00	67.67	0.00	189.92	99.96	67.41	0.00

5. RESULTS AND DISCUSSION

5.1 Generating the noisy datasets

Noise-free truth datasets were simulated for the three basic scenarios listed in Table 1. Then, pseudo-random Gaussian noises were added to the current, voltage, and temperature per the sensor specifications listed in Table 3. The "max" (and "min") entries Table 2 refer to adding (or subtracting) the dc-bias value defined by the particular sensor's specification to (from) the true value. Cases 1–4 have the effect of trying to force the SOC estimate to be greater than the truth at all times (since all profiles start in the discharge direction). Cases 5–8 bias the estimate in the other direction. These three variables are always changed together to provide \pm worst-case results.

Timing latency is assumed to impact only the voltage signal. If the latency is negative, changes to cell voltage precede changes to current and SOC (voltage is shifted left compared with other signals). If the latency is positive, voltage changes lag behind changes to current and SOC (voltage is shifted right compared with other signals).

This modified dataset is used as input to the SOC-estimation algorithms. Output SOC estimates and statistics are used as inputs to the SOH algorithms that compute resistance estimates \hat{R}_0 . The SOP-estimation algorithm is based on the nominal two R–C model, using signals from the SOC-estimation SPKF, and with R_0 replaced by $\hat{R}_0 + 3\sigma_{R_0}$ from the SOH-estimation algorithms. We evaluate results by comparing the estimated SOP to the truth SOP computed by executing the bisection method on the three R–C model and using the noise-free dataset.

5.2 Estimates of R_0

Table 4 lists numeric R_0 -estimation results, presenting RMSE between R_0 and \widehat{R}_0 for the simple and SPKF methods and listing the percentage of time that the estimator confidence bounds do not encompass the true value of R_0 . These results are similar to those presented in (Plett and McVeigh, July 2024b); however, the prior work considered sensor latencies of ± 100 ms whereas this work investigates a more realistic ± 10 ms, which is the limit of our present simulation capability.

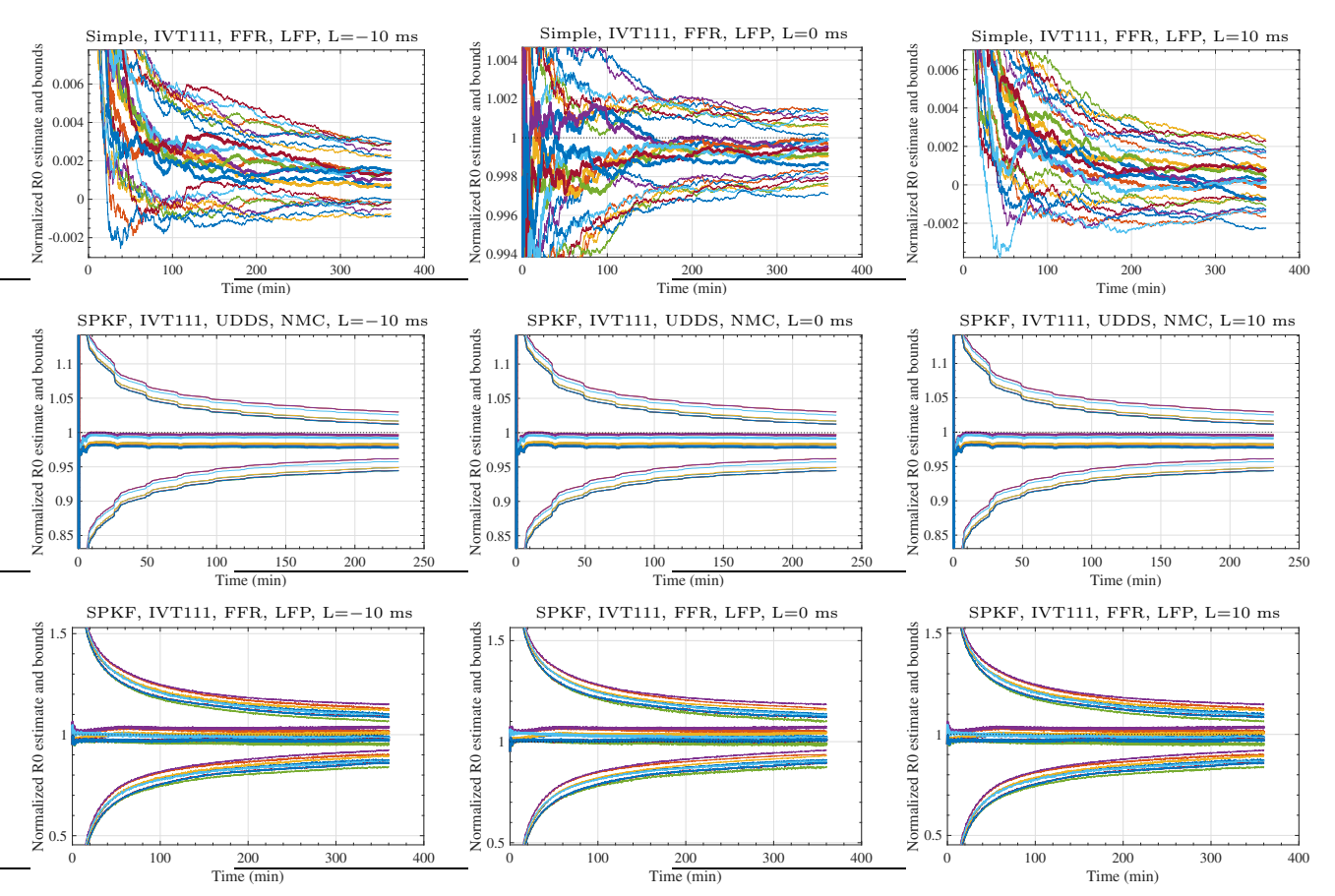


Fig. 3. Subset of resistance-estimation results, each plot for eight simulation cases for a single scenario and sensor configuration. Thick lines are estimates; thin lines of the same color are the corresponding confidence bounds.

Fig. 3 shows the evolution of normalized \widehat{R}_0/R_0 estimates over time for three example cases (the ideal result is always 1.0). Each frame shows eight thick lines illustrating \widehat{R}_0 evolving over time for the eight cases of Table 2. Thin lines of the same color draw the confidence bounds predicted by the estimator. The top row plots typical outputs from the simple method. We observe that the simple method consistently fails when there is latency between the voltage and current sensors—its estimates are close to zero since the asynchronous voltage and current signals have essentially no instantaneous correlation.

The bottom two rows of the figure illustrate typical results using the SPKF method. Because the SPKF is a filter, it provides estimates of \hat{z}_k , \hat{h}_k , and $\hat{v}_{c_i,k}$ that are reasonable, despite any timing latencies. Therefore, the overall net voltage depression caused by average current multiplied by R_0 becomes observable, whereas the simple method relies on unfiltered instantaneous changes in voltage and current. The biggest shortcoming of the SPKF method is that its confidence intervals are wide, especially for the FFR scenarios, and do not converge quickly over the course of the simulations. Given longer datasets, we believe that the SPKF method would improve its estimates and confidence windows, although this remains a topic of future work.

5.3 Estimates of SOP

Table 5 lists numeric SOP-estimation results for $T\Delta t = 10 \text{ s}$. It presents RMSE between true and estimated SOP for the bisection method based on \widehat{R}_0 estimates made by

the simple and SPKF methods; it also lists the percentage of time that SOP is overestimated.

Fig. 4 shows the evolution of the unsigned SOP estimates over time for the same examples as Fig. 3. The top row illustrates typical outputs from the simple method. When latency is nonzero, SOP is greatly overpredicted since $\widehat{R}_0 \approx 0$. Even when latency is zero, SOP is often somewhat overpredicted despite the conservative use of $\widehat{R}_0 + 3\sigma_{R_0}$ for R_0 (because σ_{R_0} is very small for the simple method).

The bottom two rows of the figure illustrate typical results using the SPKF method. SOP accuracy shows no visible degradation due to sensor latency, and very rarely overpredicts available power. Despite wide confidence bounds on \hat{R}_0 in the FFR scenario, SOP estimates are converging toward the truth by the end of the simulation.

5.4 Discussion

Studying the numeric results of Tables 4 and 5, we make several observations. All else being equal, the quality of the sensors directly impacts the RMSE of the SOP estimates. High-accuracy synchronized sensors enable high-accuracy SOP estimates that rarely overpredict true available power. Degrading any of the sensors causes a resulting degradation in the quality of the SOP estimates. Losing synchronization between voltage and current measurements is likely to degrade SOP estimates unless advanced methods (such as the SPKF approach presented here) are implemented. As a general rule, if an application

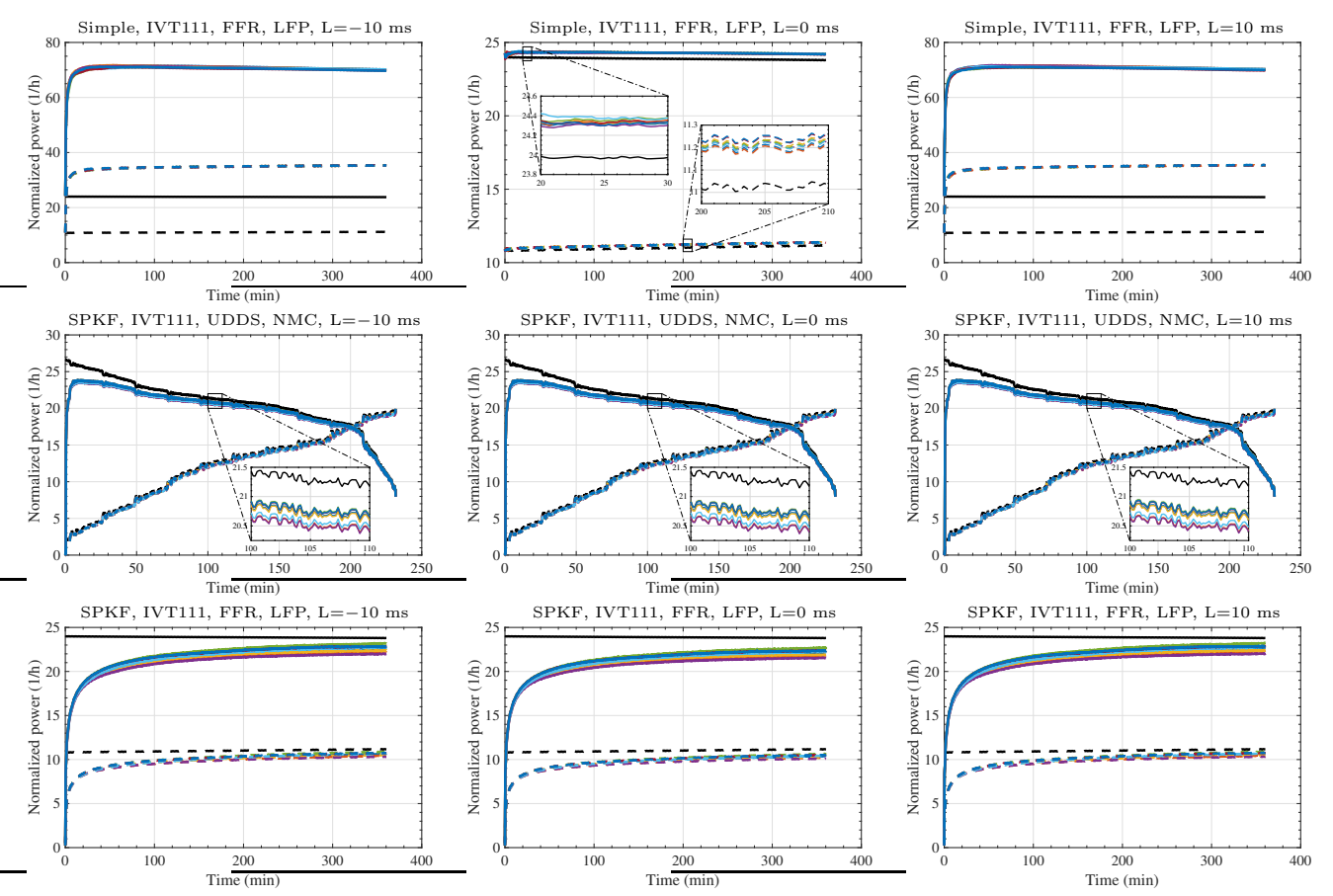


Fig. 4. Subset of unsigned SOP-estimation results, each plot for eight simulation cases for a single scenario and sensor configuration. Black line is truth; solid lines are discharge SOP and dashed lines are charge SOP. (Confidence bounds are not plotted.)

specifies a maximum permitted SOP-estimation error, this will impose requirements on the measurement error and synchronization of the sensors.

6.SUMMARY

This paper has presented a framework for evaluating the impact of sensor measurement error and synchronization latency on SOP-estimation results. It has applied that framework to a combination of scenarios encompassing automotive and energy-storage use cases for different sensor error levels and latencies. The study has confirmed in a quantitive way the intuitive expectation that better sensors enable an improvement in SOP estimation. Consequently, a BMS that uses better sensors reduces the required derating factors on those SOP metrics to compensate for poor sensing, reducing overall cost and improving sustainability and safety. This also implies that applications which specify maximum permitted SOP-estimation error will have referred requirements imposed on the quality of the sensing subsystem of the BMS. Future work might include evaluating other application profiles, different timing latencies, sensor gain errors, and the impact of cell-to-cell inhomogeneities in a battery pack for pack-level SOP estimation.

REFERENCES

Chen, C.T. (1999). Linear System Theory and Design. Oxford University Press, third edition. Plett, G.L. (2004). High-performance battery-pack power estimation using a dynamic cell model. *IEEE Transactions on vehicular technology*, 53(5), 1586–1593.

Plett, G.L. (2011). Recursive approximate weighted total least squares estimation of battery cell total capacity. *Journal of Power Sources*, 196, 2319–2331.

Plett, G.L. (2015a). Battery Management Systems, Volume 1: Battery Modeling. Artech House.

Plett, G.L. (2015b). Battery Management Systems, Volume 2: Equivalent-Circuit Methods. Artech House.

Plett, G.L. and McVeigh, G. (July 2024a). Sensitivity of lithium-ion battery SOC estimates to sensor measurement error and latency. In *Proceedings of the 4th International Conference on Electrical, Computer, and Energy Technologies (ICECET 2024)*. Sydney, Australia.

Plett, G.L. and McVeigh, G. (July 2024b). Sensitivity of lithium-ion battery SOH estimates to sensor measurement error and latency. In *Proceedings of the 4th International Conference on Electrical, Computer, and Energy Technologies (ICECET 2024)*. Sydney, Australia.

Press, W., Teukolsky, S., Vetterling, W., and Flannery, B. (1992). *Numerical Recipes in C.* Cambridge University Press, second edition.

Zeng, Y., Meng, J., Peng, J., Feng, F., and Yang, F. (2023). State of health estimation of lithium-ion battery considering sensor uncertainty. *J. Energy Storage*, 72, 108667.